Materials Today Communications 39 (2024) 108981

Contents lists available at ScienceDirect

Materials Today Communications

journal homepage: www.elsevier.com/locate/mtcomm

Effect of carbon black incorporation methods on the initial creep/slow crack growth resistance and properties of high-density polyethylene (HDPE) pipes

Seyyed-Mahdi Alavifar [a], Mahdi Salami Hosseini [a,b,*], Mir Karim Razavi Aghjeh [a,b]

[a] Polymer Engineering Faculty, Sahand University of Technology, Sahand New Town, Tabriz, Iran
[b] Institute for Polymeric Material, Sahand University of Technology, Sahand New Town, Tabriz, Iran

ARTICLE INFO

Keywords:
High-density polyethylene
Rheological analysis
Slow crack growth
Carbon black incorporation
Pipe

ABSTRACT

The increasing utilization of polyethylene (PE) pipes in diverse industries has driven a focused exploration into the properties and behaviors of PE materials. In response to this heightened interest, this study aims to investigate the impact of different carbon black (CB) incorporation methods on the properties of PE100 polyethylene, particularly its resistance to slow crack growth (SCG). Two distinct methods, direct incorporation and utilization of a commercial masterbatch, were employed to introduce CB into the PE100 matrix. Results revealed that direct incorporation led to superior dispersion of CB, thereby enhancing the mechanical properties of the resultant compound. Furthermore, SCG resistance exhibited improvement when CB was directly incorporated, contrasting with a degradation in SCG resistance observed when a CB masterbatch was used compared to neat PE. Comprehensive rheological and thermal analyses were conducted to elucidate these findings. The study concludes that the presence of low molecular weight substances and inadequate CB dispersion within the CB masterbatch significantly contributed to the deteriorated SCG resistance observed in PE100 material.

1. Introduction

Polymer-based pipes have gained preference over metal-dependent alternatives due to their numerous advantages, including adequate strength, corrosion resistance, extended cycle life, lightweight construction, and flexibility [1–4]. Among the polymers commonly employed in the pipe industry, polyethylene (PE), polypropylene (PP), and polyvinyl chloride (PVC) take the lead. PE, in particular, stands out for its exceptional properties, such as chemical resistance, high strength, suitable flexibility, stress tolerance, and leak-free performance, making it the top choice for irrigation pipes [5–8]. Within the range of PE variants, including low-density polyethylene (LDPE), linear low-density polyethylene (LLDPE), medium-density polyethylene (MDPE), and high-density polyethylene (HDPE). HDPE has emerged as the most widely utilized due to its superior crystallinity [9,10]. HDPE's structure is characterized by long linear chains with short branches, resulting in the highest crystallinity percentage among the various PE types [11]. It is well-established in the literature that higher crystallinity leads to enhanced mechanical properties in the polymer matrix, such as strength and Young's modulus [12,13].

However, one notable drawback of PE-based pipes, including HDPE, is their susceptibility to Ultraviolet (UV) radiation [14]. UV radiation can induce depolymerization reactions within the PE matrix, leading to a reduction in the molecular weight of the polymeric chains [15]. To mitigate this issue, CB is introduced to the HDPE matrix [16]. Nevertheless, the addition of carbon black can impact the final properties of the resulting pipe [17]. Typically, the inclusion of fillers in a polymer matrix reduces the crystallinity due to interface interactions between the polymer chains and the filler surface. In the case of PE chains absorbing onto the CB surface, the mobility of the PE chains becomes limited, resulting in decreased polymer crystallinity [18]. This reduction in crystallinity subsequently leads to a decline in the mechanical properties of the final product. Conversely, incorporating a filler with high mechanical strength into the polymeric matrix can enhance the overall mechanical characteristics of the composite [19]. Thus, a trade-off in the final mechanical behavior of the composite depends on the type and quantity of the filler used, as well as the state of its dispersion within the matrix [20]. The optimal carbon black content in the resultant compound, incorporated into an HDPE matrix, typically falls within the range of 2 % to 2.5 wt%. However, it is imperative to acknowledge that

* Corresponding author at: Polymer Engineering Faculty, Sahand University of Technology, Sahand New Town, Tabriz, Iran
E-mail address: salami@sut.ac.ir (M.S. Hosseini).

https://doi.org/10.1016/j.mtcomm.2024.108981
Received 10 February 2024; Received in revised form 5 April 2024; Accepted 19 April 2024
Available online 22 April 2024

the utilization of such substantial CB content can exert noteworthy influences on the rheological and mechanical characteristics of the pipe material [21,22]. One crucial property that significantly influences the long-term performance and practical lifespan of a pipe is its resistance to SCG [23]. SCG transpires as a consequence of prolonged exposure to low-intensity stresses, particularly when influenced by an active chemical agent, such as detergents. This phenomenon frequently culminates in the occurrence of brittle fractures. This process is triggered by the creation of voids, which can arise from macroscopic defects or the presence of impurities within the material mass (such as crazes and defects in the crystalline part) [24]. These imperfections and irregularities give rise to localized stress concentration. The process of SCG encompasses the stages of initiation, propagation, and eventual growth of crazes, wherein the advancement of these crazes' hinges upon the interlacing and mobility of the polymer chains. Consequently, a higher degree of chain entanglement and reduced polymer chain mobility contribute to increased SCG resistance [23,25].

Extensive research has been conducted on SCG in PE-based pipes in recent years. Favier et al. investigated slow crack propagation in PE under controlled stress intensity fatigue [26], while Haager et al. examined SCG behavior in PE following stepwise isothermal crystallization [27]. Additionally, Nie et al. developed an HDPE pipe with high SCG resistance using rotation extrusion [28], and Carlos et al. studied the effect of comonomer type on the SCG behavior of PE resins [29]. Some studies have predicted PE resin SCG resistance using the strain-hardening modulus method [30]. Deveci et al. performed both cracked round bar (CRB) and strain hardening (SH) test to study the correlation of molecular structural parameters on the SCG of PE and showed that slow crack growth resistance was better captured by SH test in comparison to CRB test [48].

However, there are limited studies that have specifically investigated the effect of carbon black on the SCG resistance of PE-based pipes. In an interesting study, Gholami et al. explored the correlation between the isothermal crystallization properties and SCG resistance of PE pipe materials manufactured using a CB masterbatch. The findings revealed that the addition of carbon black to the PE matrix decreased the SCG resistance due to CB aggregation, which acted as stress concentration regions [31].

Nevertheless, an alternative approach to manufacturing HDPE pipes involves the use of black PE granules instead of a master batch (MB) [32]. This method offers the potential for achieving better dispersion of CB within the final composite. Consequently, it becomes necessary to investigate the influence of using black PE granules on the SCG resistance of the resulting composite. In this study, we aim to investigate the effect of CB dispersion in the HDPE matrix on SCG resistance by preparing three samples. The first sample consists of pure PE granules without any carbon black (NT-PE), the second sample includes PE granules with carbon black masterbatch (MB-PE), and the third sample incorporates black PE granules (BK-PE). The dumbbell-shaped samples are produced using an internal mixer and a hot press. Subsequently, we will analyze the dispersion of CB in the final composite, examine the crystalline behavior, assess the mechanical and rheological properties, and evaluate the SCG resistance of the resulting compounds.

By systematically studying the impact of carbon black dispersion on SCG resistance, this research aims to provide valuable insights into the design and optimization of PE-based pipes. The findings will contribute to the development of improved pipe manufacturing techniques, enhancing the durability and long-term performance of PE pipes in various applications. Additionally, this study will advance the understanding of the relationship between filler dispersion, crystalline behavior, and mechanical properties in polymer composites, shedding light on the fundamental aspects of composite material design and performance.

Overall, this research presents a comprehensive investigation of the influence of CB incorporation on the SCG resistance of HDPE-based pipes. The outcomes will serve as a valuable resource for researchers, pipe production companies, and industry professionals involved in the design, development, and application of polymer-based pipes.

2. Materials and methods

2.1. Materials and sample preparation

2.1.1. Materials

High-density polyethylene, HDPE, (HD-EX3–100) with MFI of 0.22 g/10 min (190°C, 5 kg) and 2.6 g/10 min (190 °C, 21.6 kg) was obtained from Maroon Petrochemical Co. A carbon black masterbatch comprising HDPE with a CB content of 40 % (Kimcol 5851) was purchased from Kimia Javid Sepahan Co. and employed as the source of CB. Moreover, black HDPE (HD-EX3–100B, by Maroon Petrochemical Co.) with the same properties as HDPE containing 2.25 %±0.25 % of carbon black was utilized. Octylphenoxypolyethoxyethanol (Igepal CO-630, Sigma-Aldrich Co.) was used as received as the nonionic surfactant in the SCG test.

2.1.2. Samples preparation

All samples including neat PE (NT), black PE (BK) and PE/CB-Masterbatch (MB) underwent a controlled mixing process for 6 minutes at 210 °C in an internal mixer and speed of 60 rpm (Brabender W50EHT, Germany). Resulting compounds were transferred into the appropriate dumbbell shape mold, as ISO 16770 proposed, in a hot press (Brabender Polystat 200 T, Germany) and compressed at 210 °C and 100 bar for 2 minutes, following 4 minutes of cooling. Notches and perforations were made for the purpose of investigating creep behavior according to ISO 16770 (Fig. 1). Equally rigorous procedures were applied for the preparation of the strain hardening (SH) test specimens in obedience of ISO 18488. The molten compounds were compression molded to form sheets with thickness of 0.3 mm, and were cut using a punch knife into proper dumbbell shape according to ISO 18488 standard. This methodical approach guaranteed precision in both testing and specimen preparation.

2.2. Microscopical observations

The evaluation of the filler distribution within samples, namely MB-PE and BK-PE, was performed employing AHP Plastic Makina Dispersion Tester, a specialized optical microscope equipped with an image analyzing software. In accordance with the ISO 18553, minute sections were judiciously extracted from the samples and meticulously clamped between two glass slides and the assembly was subjected to controlled thermal exposure surpassing the sample's melting point (180 °C) for a duration of 10 min within a controlled-temperature oven. Subsequent microscopic examinations discerned the intricate dissemination pattern of diminutive filler particles, thereby affording valuable insights into the dispersion characteristics of the samples. To examine the fracture interface of the samples, a Field-Emission Scanning Electron Microscopy (TESCAN MIRA3 FE-SEM, Czech Republic) was utilized.

2.3. Thermal analysis

To evaluate the crystallinity and thermal properties, a differential scanning calorimetry (DSC) apparatus, NETZSCH DSC 200 F3 Naia manufactured by Netzsch, Germany, was employed. DSC test was conducted in three stages: heating, cooling, and reheating, covering a temperature range from 25 °C to 250 °C and vice versa, under a nitrogen atmosphere with a heating and cooling rate of 10 °C/min. The primary heating stage aimed to eliminate the sample's thermal history, followed by the subsequent cooling and secondary heating stages.

2.4. Strain hardening test

In an endeavor to meticulously investigate and draw comparisons

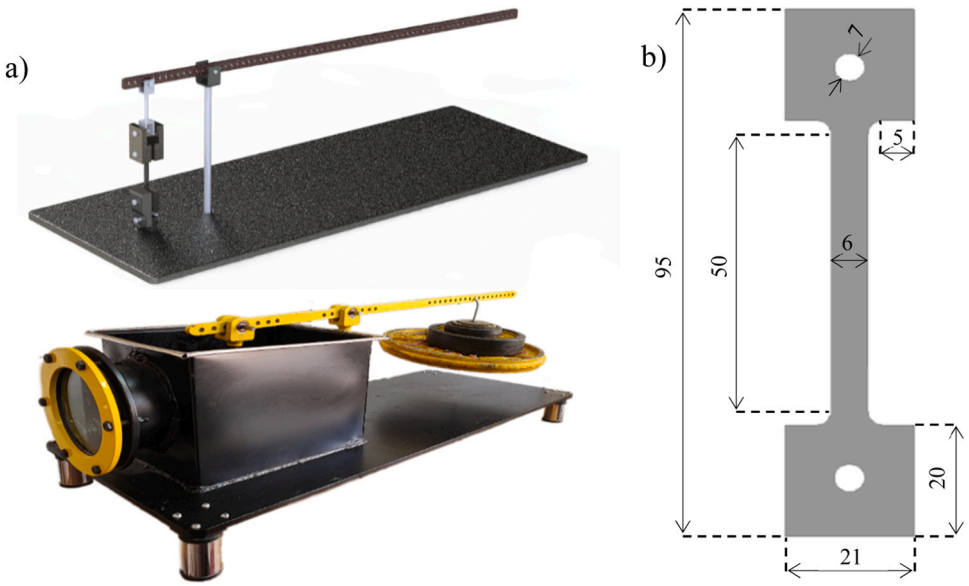

Fig. 1. Overview of a) designed device and b) the creep test sample.

among the mechanical attributes exhibited by the specimens, a Zwick/Roell Z010 tensile testing apparatus, manufactured by Zwick/Roell, was enlisted. The conducted tensile assessments were carried out with an applied strain rate fixed at 20 mm/min, all conducted at ambient temperature (23 °C) in accordance with ISO 18488 guidelines. Ensuring the integrity of the collected data, each specimen underwent three separate test iterations, with the resulting values then subjected to meticulous averaging procedures.

2.5. Rheological measurements

Rheological analysis was carried out utilizing a dynamic rheometer (Anton Paar MCR301) equipped with a parallel plate featuring a 25 mm diameter and the uniform gap of 1 mm. Dynamic frequency sweep experiments were conducted with precision over the angular frequency range of 0.01–628 rad/s. All tests were conducted under controlled thermal conditions at a temperature of 190 °C a. The 1.0 % strain amplitude was chosen after a strain sweep test, aiming to constrain the material's response within the linear viscoelastic region.

2.6. Creep Test

To assist the evaluation of the slow crack growth resistance of the specimens, a creep testing apparatus adhering to the ISO 16770 standard (as depicted in Fig. 1) was employed. Furthermore, in order to expedite the propagation of cracks and the onset of failure mechanisms, the dumbbell-shaped specimens were completely immersed in the 2 wt% aqueous solution of Igepal CO-630, replicating an aggressive environmental condition stipulated by ISO 16770 during the testing procedure. The test was carried out at room temperature (25 °C) with a dead load stress of 9 MPa.

2.7. Data accuracy checking

To ensure the precision and reliability of data and enable rigorous comparisons among three distinct sample types, a one-sided analysis of variance (ANOVA) was conducted. The utilization of ANOVA served the purpose of validating data comparability across these diverse sample types. A significance level of 0.05 and a 95 % confidence interval were employed, with the resultant p-value from this analysis serving as an indicator of statistical significance. A p-value exceeding 0.05 indicates that parameter values among the sample types are statistically similar, whereas a p-value below 0.05 signifies the presence of significant differences among them.

3. Result and discussion

3.1. Carbon black dispersion

Prior to examining the SCG proclivities observed in the fabricated specimens, it is imperative to conduct an assessment of the dispersion of CB within the HDPE matrix. This assessment applies to both the MB-PE and BK-PE samples. Fig. 2 shows the result of the CB dispersion evaluation in the HDPE matrix for MB-PE and BK-PE samples. Fig. 2a to b show the micrograph of MB-PE while Fig. 2c and d represent that for BK-PE. It can be seen that CB dispersion was visually much better in BK-PE compare to MB-PE. The result of image analysis and using normal distribution the particle size distribution for both samples were plotted and portrayed in Fig. 2e. Carbon black particles have a tendency to aggregate because of their active surfaces, making it hard to evenly spread them in a matrix [33]. So, it's challenging to achieve a good dispersion of CB when using a masterbatch. However, in the BK-PE sample, a better and more even dispersion of CB was observed within the HDPE matrix, resulting in smaller particle sizes. This can be attributed to the better mixing capabilities in direct incorporation of CB due to the low initial concentration of CB and absence of wax and similar processing aids used in incorporation of high CB concentration. As it was reported in Table 1, the average particle sizes for MB-PE and BK-PE were 16.90 ± 12.19 μm and 7.75 ± 2.39 μm, respectively. The statistical analysis indicated a significant difference between these two samples, with a p-value of zero at a significance level of 0.05 (Table 1). Furthermore, in the MB-PE sample, the distribution of carbon black particles was uneven, suggesting the presence of impurities such as zinc, calcium stearate, and wax used as processing aids in preparation of CB masterbatch [22,34]. These impurities could introduce detrimental effects on the mechanical properties and crystalline behavior of the HDPE which will be discussed in next sections.

3.2. Crystallinity and thermal properties

Fig. 3 exhibits the Differential Scanning Calorimetry (DSC) thermograms and cumulative heat flow profiles for all samples. The data presented in Figs. 3a and 3b indicate a substantial reduction in the melting peak of HDPE upon the introduction of carbon black into its matrix. For

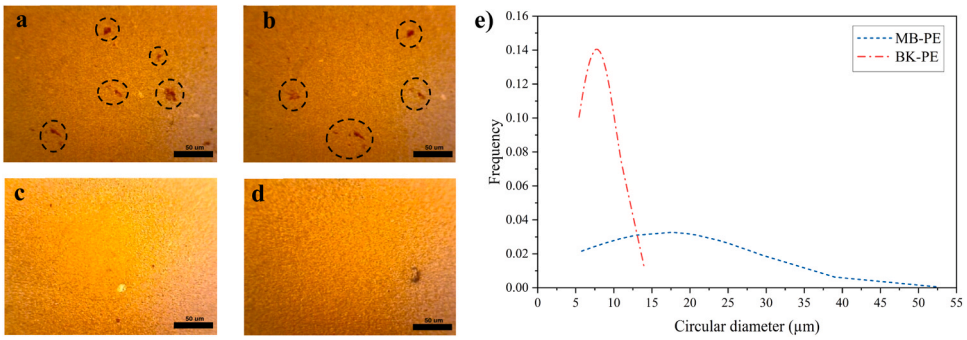

Fig. 2. Optical microscopic images of MB-PE (a and b), BK-PE (c and d) and CB particle size distributions for MB-PE and BK-PE(e).

Table 1
Average CB particle sizes of the samples.

Property	MB-PE	BK-PE	p-value
CB average diameter(m)	16.90±12.19	7.75±2.39	<0.001

a quantitative evaluation of crystallinity, Table 2 provides the computed crystallinity values for each sample, including NT-PE, BK-PE, and MB-PE, yielding values of 53.75±0.78, 51.97±0.31, and 49.76±0.65, respectively. The calculated p-value of the data showed a statistically significant difference in the crystallinity of the samples. The integration of CB into the polymer matrix initiated a sequence of interactions leading to the adsorption of polymeric chains onto the surface of CB, thereby instigating a constraining effect on the mobility of the polymer chains [34]. Consequently, this phenomenon induces a conspicuous reduction in the polymer's crystallinity, a phenomenon consistently corroborated by previous findings [21,35,36]. It is noteworthy that the outcomes align closely with the anticipated decrease in crystallinity for both BK-PE and MB-PE samples, thus validating the initial expectations. However, a closer examination revealed that the BK-PE sample experienced a relatively lesser decrease in crystallinity compared to the MB-PE sample. As mentioned earlier, carbon black, as a dispersed phase, could function as a nucleating agent for polymer crystallization [22]. Furthermore, an improved dispersion of CB characterized by smaller particle dimensions was observed within the BK-PE sample, enhancing its nucleation potential. Consequently, the BK-PE sample demonstrated a diminished reduction in crystallinity, attributable to the abundant presence of nuclei facilitated by the more effective dispersion of CB, in contrast to MB-PE. This observation is substantiated by the comparison of crystallization onset. As reported in Table 2, the onset of crystallization for BK-PE was recorded at 117.10 °C, surpassing that of MB-PE at 116.55 °C, indicating a slightly higher level of nucleation in the case of BK-PE owing to the suitable dispersion of CB in PE matrix.

The crystalline characteristics observed within polymers are inherently determined by the structural attributes of polymer chains and their intermolecular interactions [37]. In light of the fact that the introduction

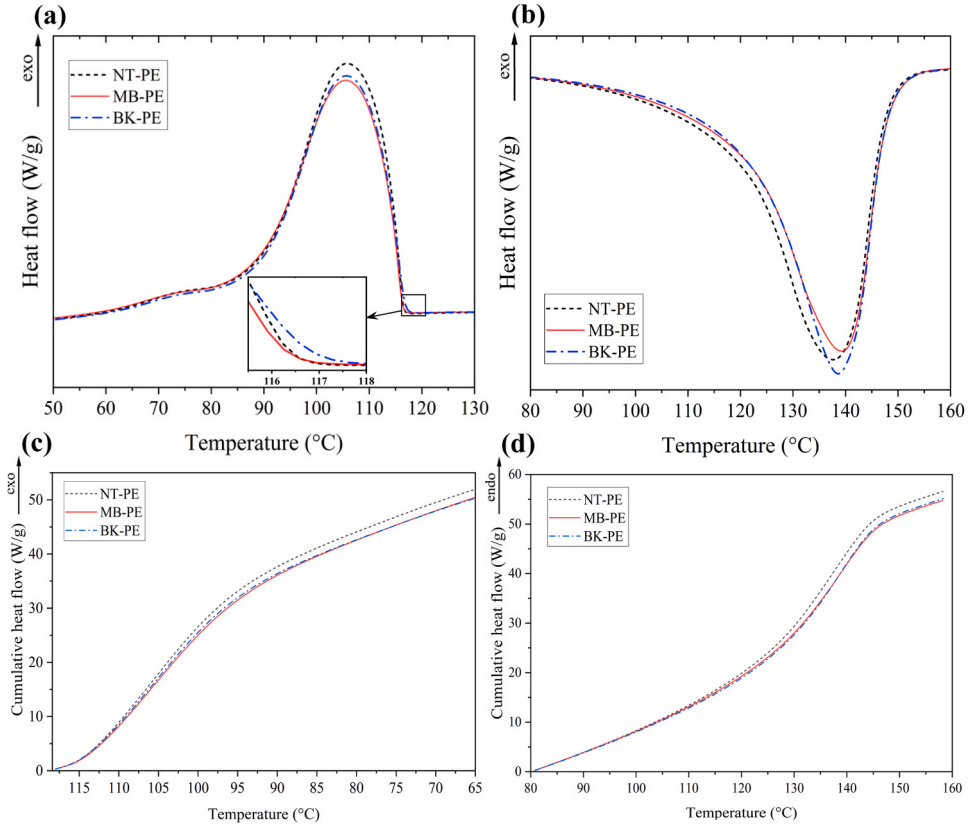

Fig. 3. Heating (a) and cooling (b) curves and cumulative enthalpy of crystallization (c) and melting (d) curve of the samples.

Table 2
Thermal properties of the samples.

	Property	NT-PE	MB-PE	BK-PE	p-value
Thermal properties	Crystallinity (%)	53.75 ±0.78	49.76 ±0.65	51.97 ±0.31	0.044
	Melting temperature (℃)	137.45 ±0.25	138.01 ±1.40	138.55 ±0.05	0.676
	Crystalline temperature (℃)	105.15 ±0.45	106.30 ±0.08	105.81 ±0.20	0.595
	Crystallization onset (℃)	116.15 ±0.21	116.55 ±0.07	117.10 ±0.14	0.019

of CB did not yield any discernible alterations in the chain structure or crystal type of HDPE, it was reasonable to anticipate that the melting and crystallization temperatures would remain unaltered, as previously indicated [21,36]. As depicted in Table 2, the melting and crystallization temperatures demonstrate minimal discrepancies across the various sample types. Utilizing analysis of variance with a significance level of 0.05, the computed p-values for melting and crystallization temperatures were found to be 0.676 and 0.595, respectively, both surpassing the specified significance threshold. Consequently, no statistically significant variations in either melting or crystallization temperatures were discerned among the examined samples. Hence, it could be deduced that the incorporation of CB into the PE structure did not elicit appreciable alterations in these thermal properties.

Fig. 3c and d shows the cumulative enthalpy of the samples derived from DSC thermograms for crystallization and melting, respectively. In Fig. 3c, the slopes of the cumulative enthalpy of crystallization for MB-PE and BK-PE were almost the same, indicating comparable crystallization and melting rates. In contrast, the filler-free NT-PE sample exhibited a higher slope both in crystallization and melting. Fig. 3c suggests an increased crystallization rate compared to the filler-containing samples. It can be concluded that the inclusion of CB particles within PE would suppress the mobility of PE chains, impending their progression towards crystalline structure. As a result, this phenomenon would engender decelerated crystallization rates, leading to comparatively decreased crystallinity when it juxtaposed with NT-PE. The cumulative enthalpy of melting (Fig. 3d) indicates that the NT-PE sample had a steeper slope compared to the other samples, indicating a higher melting rate. It can be attributed to the more uniform crystal structure in the NT-PE sample, facilitating an accelerated melting process compared to MB-PE and BK-PE.

3.3. Mechanical properties

Fig. 4 shows the stress verses strain curve for all samples and the resultant mechanical properties including Young's Modulus, tensile strength and elongation at break of the samples were summarized in Table 3. It can be seen from Fig. 4 that all samples tend to reach a certain yield stress and then fall to a plateau region followed by a strain-hardening behavior. Comparing the yield stress (τ_y) and elongation at break (ε_b) of the samples, as inferred from the p-values analysis, suggested that the introduction of carbon black (CB) did not impart a statistically significant effect on both τ_y and ε_b. Conversely, the Young's modulus (E) and tensile strength (τ_b) undergo a notable alteration following the incorporation of CB into polyethylene (PE), as

Table 3
Mechanical properties of the samples.

	Property	NT-PE	MB-PE	BK-PE	p-value
Mechanical properties	Yield stress (MPa)	21.1 ±0.25	21.3 ±0.21	20.7 ±0.33	0.152
	Young's Modulus (MPa)	1226 ±44.62	1105 ±68.75	1510 ±59.16	0.001
	Ultimate strength (MPa)	29.4 ±0.34	27.4 ±0.54	31.2 ±0.45	0.001
	Elongation at break (%)	931 ±33.51	934 ±43.68	949 ±45.37	0.902

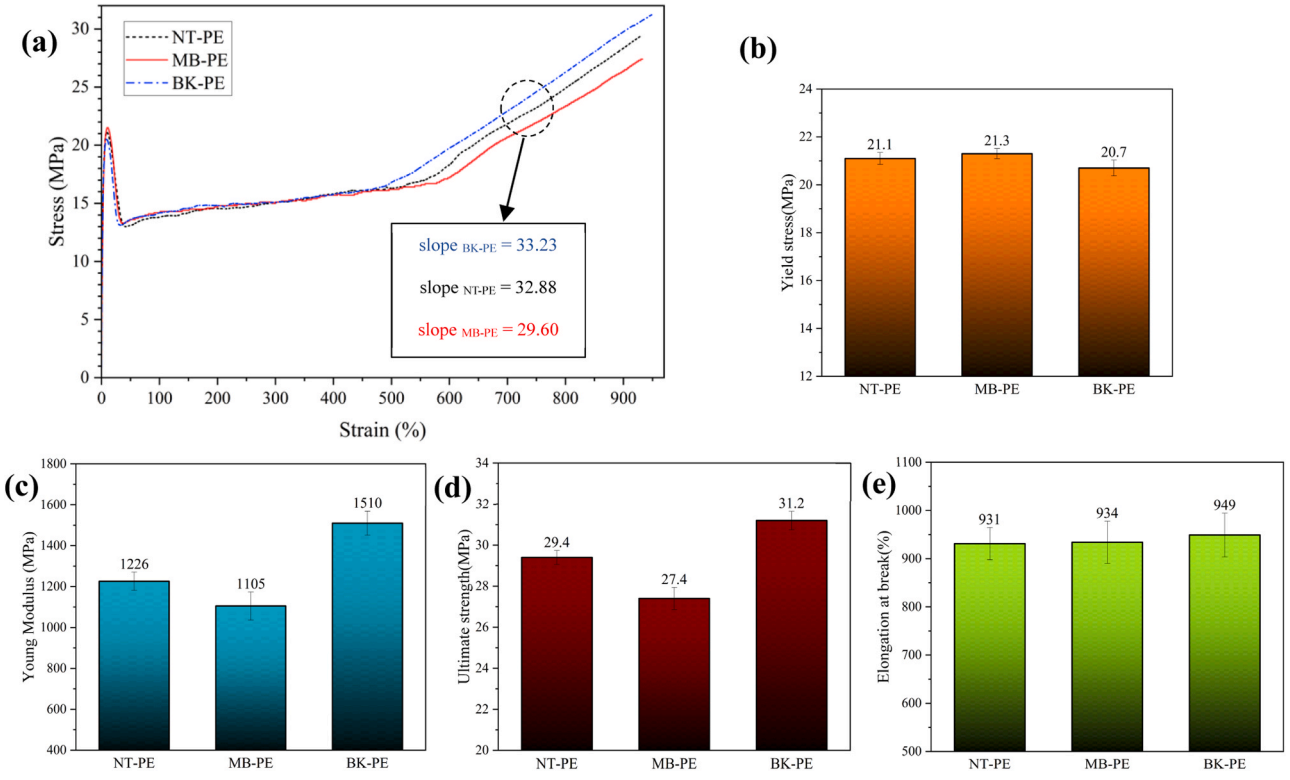

Fig. 4. (a)Stress-strain curves, (b) yield stress, (c) Young's modulus, (d) ultimate strength, and (e) elongation at breaks of the samples.

substantiated by the calculated p-values. The Young's modulus was measured as 1226 MPa for NT-PE while decreased to 1105 MPa for MB-PE and increased to 1510 MPa for BK-PE. The same trend was also observed in the case of tensile strength. The observed decrease in mechanical properties of MB-PE can be attributed to the combination of different factors. These include inadequate dispersion of carbon black (CB), reduced interaction between CB and PE, and the presence of low molecular weight impurities such as waxes, processing aids, and lubricants (Scheme 1). It can be postulated that the presence of low molecular weight impurities could result in reduction of Young's modulus as described by the mixture law. Conversely, the BK-PE sample displayed an opposing trend, with increased tensile strength and Young's modulus. This observation can be attributed to the improved dispersion of carbon black, as depicted in Fig. 2 and visually described in Scheme 1, which enhances the interaction between CB and PE by increasing the contact surface area of CB/PE. Additionally, the absence of low molecular weight components, as CB is directly incorporated at lower concentrations into the PE, results in superior CB dispersion and higher tensile strength and Young's modulus.

In the stress-strain curve (Fig. 4), the increasing slope in the post-yield region indicates strain hardening phenomenon (SH), characterized by aligned polymer chains and the formation of new crystals [38,39]. The strain hardening (SH) modulus was determined for each sample, resulting in the values of 32.88, 33.23, 29.60 for NT-PE, BK-PE, and MB-PE, respectively. Notably, the BK-PE sample displayed a substantial enhancement in SH modulus, underscoring the positive impact of the CB filler on tensile strength. This effect can be attributed to the effective and uniform dispersion of CB particles, which significantly restricts chain mobility within the polymer matrix [18]. The SH modulus of the MB-PE sample was found to be reduced at 29.60. This decrease could be ascribed to the interference caused by the presence of small molecules, which acted as plasticizers and hindered the entry of polymer chains into crystalline structures. This finding is consistent with the crystallinity data presented in Table 2.

Moreover, the BK-PE sample displayed an accelerated initiation of strain hardening, a phenomenon facilitated by the even dispersion of CB particles and the alignment of polymer chains. With increased interaction of CB due to the better dispersion, the CB fine particles (or better say aggregates, could act as physical bonders forming an integrated structure in BK-PE sample inducing earlier initiation of SH. In contrast, the MB-PE sample showed a delayed onset of strain hardening, which can be attributed to hindered chain alignment due to the presence of small molecules and, as mentioned earlier, inadequate CB dispersion.

3.4. Rheological properties

In Fig. 5a, storage modulus (G′) and complex viscosity (η*) are plotted against angular frequency (ω) for all three samples. It is evident that at higher frequencies, G' and η* converge to almost similar values, following the same trend across all samples. This outcome was anticipated, given that the base matrix of the samples was the same, and it is widely recognized that the behavior of G' and η* at high frequencies is primarily determined by the flow-induced molecular orientation of the matrix [40], However, a slight reduction in G′ at higher frequencies was observed in the case of MB-PE. This observation can be ascribed to the presence of lower molecular weight components within the used masterbatch. At midrange and low frequencies, both MB-PE and BK-PE demonstrated higher G′ values compared to NT-PE, with BK-PE exhibiting the highest G′. This can be attributed to the incorporation of carbon black (CB) into the PE matrix, resulting in increased values for both G′ and η* at midrange and low frequencies, as expected due to the introduction of the elastic component, CB, in this case. As it was discussed earlier, BK-PE had a better CB dispersion compare to MB-PE sample. This, in turn, could facilitated the formation of a three-dimensional network resulting from the CB and PE interaction. This phenomenon was reflected in the increase of storage modulus at lower frequencies for BK-PE. In case of MB-PE, due to the inadequate CB dispersion and also the presence of lower molecular weight components in CB masterbatch, the elasticity was lower than that for BK-PE at lower frequencies.

Fig. 5b illustrates the van Gurp-Palman plot of the samples, plotting the phase angle (δ) against complex modulus (G*). NT-PE displayed an inflection from 90° at lower values of G*, indicative of a bimodal molecular weight distribution, consistent with the characteristics of the PE grade used (PE100) [41,42]. Upon the introduction of CB into the PE matrix, an amplified deviation was observed, with BK-PE exhibiting more pronounced elasticity compared to MB-PE. This can be also attributed to the superior CB dispersion in BK-PE, as discussed earlier. The Cole-Cole plots (η'' vs. η') for the samples are presented in Fig. 6. It was expected that NT-PE, as a single-phase material, would exhibit a semi-circular shape, however, despite conforming to the semi-circular trend at higher frequencies (low η'' and η'), it deviated by displaying a tail at lower frequencies (high η'' and η'). This behavior can be due to the pronounced entanglement of high molecular weight polyethylene chains in PE100 resins [43]. This interpretation was further corroborated by the weighted relaxation time spectrum data presented in Fig. 7, revealing a terminal tail at longer relaxation times (λ) for NT-PE due to the aforementioned entanglements. Additionally, this speculation also found validation in the slope of G′ vs. ω at low frequencies, which was measured as 0.90, 0.74, and 0.65 for NT-PE, MB-PE, and BK-PE, respectively (Fig. 5a). These values were notably distinct from the

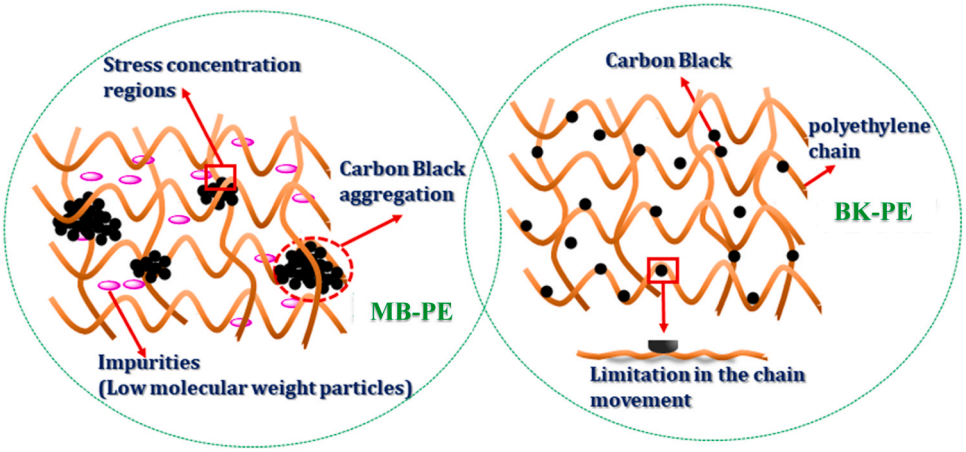

Scheme 1. A schematic representation of CB dispersion and interaction in MB-PE and BK-PE.

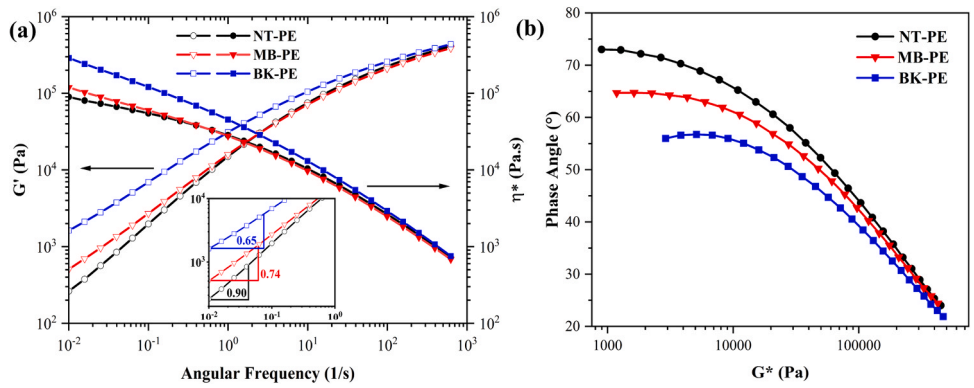

Fig. 5. (a) G' and η* vs angular frequency and (b) the van Gurp-Palman plot of NT-PE (●), MB-PE (▼), and BK-PE (■).

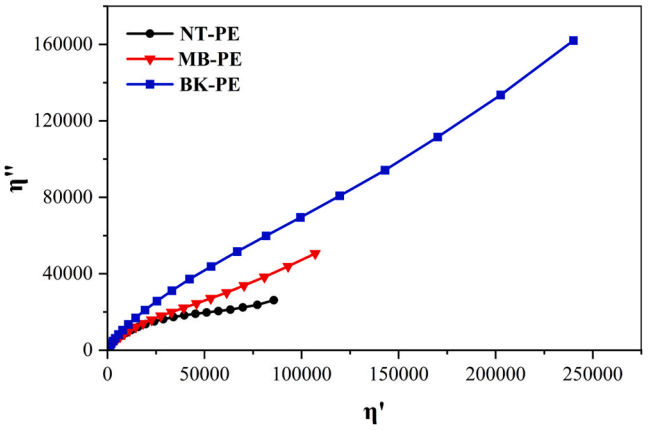

Fig. 6. The Cole-Cole plots (η'' vs. η') of NT-PE (●), MB-PE (▼), and BK-PE (■).

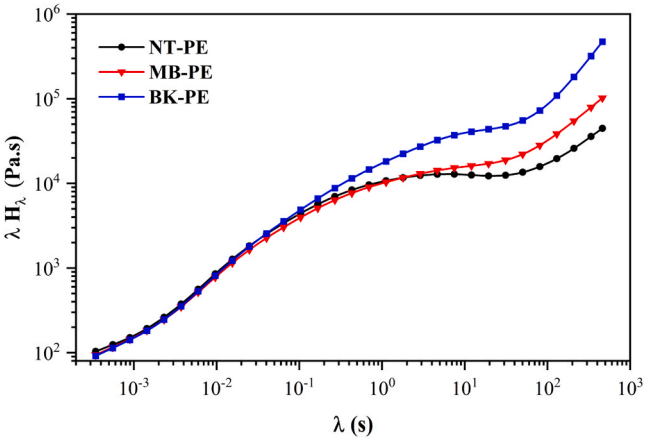

Fig. 7. Relaxation spectrum (λH(λ) vs. λ) of NT-PE, MB-PE, and BK-PE.

expected value of 2 for a typical isotropic polymer melt. Similarly, Fig. 5a depicted a pronounced deviation from the semi-circular shape for MB-PE and BK-PE, which could be associated with the incorporation of CB and the state of CB dispersion within the matrix, as discussed earlier. Moreover, the weighted relaxation spectrum of MB-PE and BK-PE exhibited higher values of λH(λ) at extended relaxation times (λ) and featured a pronounced terminal tail, signifying the presence of an additional relaxation mechanism resulting from the interaction of CB with the PE matrix in MB-PE and BK-PE samples (Fig. 7).

3.5. Slow crack growth (SCG) resistance

Results of the creep test of the samples, ε vs. t, are presented in Fig. 8 and final failure time of the samples are reported in Table 4. It was noted that samples exhibited a power-law behavior in creep test, and the power-law coefficients for each sample are listed in Table 5. Evidently, the MB-PE sample displayed the shortest failure time of all samples about 10 h followed by NT-PE and BK-PE which exhibited failure times of roughly 18 and 21 h, respectively. Notably, the p-value computed from the results in Table 4 indicates that it was well below the significance level of 0.05 showing a statistically significant difference in the final failure times. The well-dispersed carbon black in the BK-PE sample facilitated the enhanced adsorption of PE chains onto the CB particles, resulting in a delayed disentanglement of PE chains and leading to a prolonged and additional relaxation process, as depicted in Fig. 4 and previously reported in [23]. The power-law index of BK-PE (0.5244) in Table 5, shows that BK-PE has the lowest rate of strain confirming the previous postulation. Conversely, the MB-PE sample demonstrated the highest power-law index among the samples, measuring 0.7015, and failure time of, approximately, 10 h showing a significant reduction in SCG resistance compare to NT-PE with failure time of about 18 and power-law index of 0.6793. This observation can be attributed to a dual causal influence, arising from the dispersion state of filler particles within the PE matrix and the presence of low molecular weight components. In Fig. 2, it is evident that the inadequate dispersion of CB

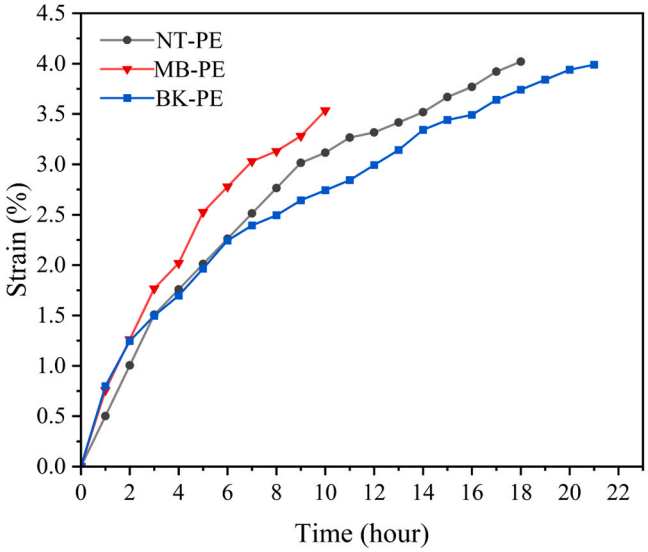

Fig. 8. Creep test curves (strain vs. time) for NT-PE (●), MB-PE (▼), and BK-PE (■).

Table 4
Failure time of prepared samples.

Property	NT-PE	MB-PE	BK-PE	p-value
Failure time (h)	17.6±1.7	10.3±1.2	20.6±2.5	0.004

Table 5
Power-law index of creep test results for the samples.

Property	NT-PE	MB-PE	BK-PE	p-value
Power-law index	0.7015	0.6793	0.5244	0.004

within the polyethylene matrix, in case of MB-PE, leads to the formation of CB agglomerates. These agglomerates have the potential to hinder the adsorption of PE chains onto the CB particle surfaces, thereby impeding the intermolecular interactions between PE chains and CB particles. Besides, the low molecular weight components such as wax and lubricants can easily reside between polymer chains in amorphous regions, facilitating their mobility and leading to a more facile disentanglement. Consequently, the amorphous regions situated between the crystalline layers [44], which correspond to the crack propagation path, exhibit reduced strength, resulting in more effortless crack propagation compared to other samples.

Previous investigations have already suggested a potential association between the slope of the stress-hardening (SH) region in the stress-strain curve and a material's resistance to stress corrosion cracking (SCG) as well as its time to failure in creep testing [45–47]. A steeper slope within the SH region signifies a heightened resistance to SCG. This behavior is ascribed to the increased entanglement and enhanced intermolecular interactions, which in turn result in a more robust amorphous phase and well-defined crystalline regions. The findings from this study reveal that the BK-PE sample exhibits the highest SH slope, whereas MB-PE demonstrates the lowest, with NT-PE falling in between. Notably, the hierarchy of slope values mirrors the time to failure observed in the creep test, thus underscoring a discernible correlation between the two phenomena. These results underscore the significance of the SH region characteristics in bolstering resistance to stress corrosion cracking during creep testing.

Fig. 9 illustrates the fracture surface morphology as observed through field-emission scanning electron microscopy (FE-SEM) for the tested samples. A distinct contrast in fracture surface characteristics is evident between BK-PE and the remaining specimens. Specifically, BK-PE exhibits a notably rougher fracture surface replete with a profusion of wrinkles, indicative of the presence of numerous sites of deformed surfaces and shorter fibrils. These observations align with the expected outcome resulting from the heightened interaction between carbon black (CB) and polyethylene (PE) in the BK-PE sample. In contrast, both MB-PE and NT-PE present fracture surfaces that bear striking similarities, characterized by longer and coarser fibrils. The structural resemblance between these two specimens implies that, in the case of MB-PE, CB exhibits a relatively diminished interaction with PE. It is noteworthy that, despite the presence of CB, the influence of low molecular weight constituents becomes discernible, as evidenced by the formation of elongated and coarser fibrils, akin to those observed in NT-PE. Thus, the FE-SEM images provide the visual evidence that supports the findings obtained from the creep test.

4. Conclusion

In summary, the present study has unveiled a clear relationship between the dispersion state of carbon black (CB) and the slow crack growth (SCG) properties of the tested samples. It is concluded that an enhanced CB dispersion results in improved SCG resistance, characterized by prolonged failure times. It is essential to note that the method of CB incorporation into polyethylene (PE) exerts a profound influence on SCG resistance. Direct CB incorporation yielded a notable enhancement in SCG resistance, whereas the introduction of CB via a concentrated carrier (masterbatch) was associated with diminished SCG resistance due to inadequate CB dispersion and the presence of lower molecular weight components such as lubricants and wax. These conclusions found substantial support in various test results.

Furthermore, the rheological analyses of the samples illuminated the underlying mechanisms. CB furthered the development of a network within the amorphous state, particularly at low shear rates, thereby fortifying SCG resistance. Nevertheless, the presence of low molecular weight constituents was shown to have an adverse impact on SCG resistance. Additionally, the slope of the strain-hardening region in the

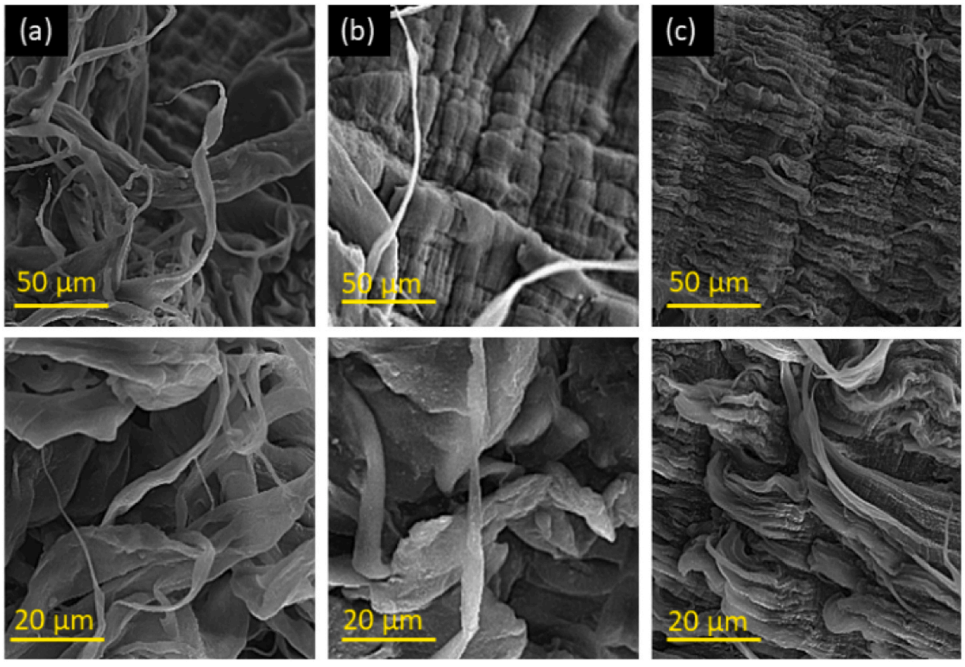

Fig. 9. Impact test fracture surface FE-SEM images for (b) NT-PE, (c) MB-PE, and (d) BK-PE.

stress-strain curve stood out as a direct indicator of SCG resistance, with higher slopes indicative of superior SCG resistance.

These findings collectively underscored the multifaceted interplay of CB dispersion, CB incorporation methods, and rheological properties in shaping SCG resistance. They provided valuable insights for the design and development of advanced materials with enhanced resistance to slow crack growth, thereby fostering improved material durability in practical applications.

Declaration of Competing Interest

Hereby, the authors declare no conflicts of interest associated with this research work. This study was conducted impartially and without influence from any external affiliations, financial interests, or personal relationships that could potentially bias the findings or interpretations presented in this manuscript. The authors affirm that the research was conducted with the highest ethical standards and scientific integrity.

Data availability

Data will be made available on request.

References

[1] S. Lyu, C. Wang, C. Zhang, L. Royon, X. Guo, Experimental characterization of a novel soft polymer heat exchanger for wastewater heat recovery, Int. J. Heat. Mass Transf. 161 (2020) 120256.

[2] C.Y. Khripin, J.A. Fagan, M. Zheng, Spontaneous partition of carbon nanotubes in polymer-modified aqueous phases, J. Am. Chem. Soc. 135 (18) (2013) 6822–6825.

[3] J.A. Harrington, A review of IR transmitting, hollow waveguides, Fiber Integr. Opt. 19 (3) (2000) 211–227.

[4] Messina, N., Colladon, M., Fossati, P., & Meynet, C. (2015, October). Internal lining of carbon steel flowlines with a plastic liner based on a fluorinated polymer: introduction of the concept and evidences on CAPEX and OPEX Reductions. In: Proceedings of the Offshore Technology Conference Brasil (p. D021S023R001). OTC.

[5] P.J. DesLauriers, M.P. McDaniel, D.C. Rohlfing, R.K. Krishnaswamy, S.J. Secora, E. A. Benham, B.B. Beaulieu, A comparative study of multimodal vs. bimodal polyethylene pipe resins for PE-100 applications. Polym. Eng. Sci. 45 (9) (2005) 1203–1213.

[6] H. Narei, M. Fatehifar, R. Ghasempour, Y. Noorollahi, In pursuit of a replacement for conventional high-density polyethylene tubes in ground source heat pumps from their composites–a comparative study. Geothermics *87* (2020) 101819.

[7] L.K. Nguyen, S. Na, Y.G. Hsuan, S. Spatari, Uncertainty in the life cycle greenhouse gas emissions and costs of HDPE pipe alternatives, Resour., Conserv. Recycl. 154 (2020) 104602.

[8] L. Nguyen, G.Y. Hsuan, S. Spatari, Life cycle economic and environmental implications of pristine high density polyethylene and alternative materials in drainage pipe applications, J. Polym. Environ. 25 (2017) 925–947.

[9] A. Frank, G. Pinter, R.W. Lang, Prediction of the remaining lifetime of polyethylene pipes after up to 30 years in use, Polym. Test. 28 (7) (2009) 737–745.

[10] Morshedian, J., & Mohammad, H.P. (2009). Polyethylene cross-linking by two-step silane method: a review.

[11] X.M. Zhang, S. Elkoun, A. Ajji, M.A. Huneault, Oriented structure and anisotropy properties of polymer blown films: HDPE, LLDPE and LDPE, Polymer 45 (1) (2004) 217–229.

[12] B. Crist, C.J. Fisher, P.R. Howard, Mechanical properties of model polyethylenes: tensile elastic modulus and yield stress, Macromol. 22 (4) (1989) 1709–1718.

[13] G. Sui, W.H. Zhong, X. Ren, X.Q. Wang, X.P. Yang, Structure, mechanical properties and friction behavior of UHMWPE/HDPE/carbon nanofibers, Mater. Chem. Phys. 115 (1) (2009) 404–412.

[14] Y. Javadi, M.S. Hosseini, M.K.R. Aghjeh, The effect of carbon black and HALS hybrid systems on the UV stability of high-density polyethylene (HDPE), Iran. Polym. J. 23 (2014) 793–799.

[15] B. Singh, N. Sharma, Mechanistic implications of plastic degradation, Polym. Degrad. Stab. 93 (3) (2008) 561–584.

[16] J.E. Weinstein, B.K. Crocker, A.D. Gray, From macroplastic to microplastic: degradation of high-density polyethylene, polypropylene, and polystyrene in a salt marsh habitat, Environ. Toxicol. Chem. 35 (7) (2016) 1632–1640.

[17] A.K. Sahu, K. Sudhakar, R.M. Sarviya, Influence of UV light on the thermal properties of HDPE/Carbon black composites, Case Stud. Therm. Eng. 15 (2019) 100534.

[18] Y. Li, M. Kröger, W.K. Liu, Nanoparticle effect on the dynamics of polymer chains and their entanglement network, Phys. Rev. Lett. 109 (11) (2012) 118001.

[19] M.H. Al-Saleh, U. Sundararaj, Review of the mechanical properties of carbon nanofiber/polymer composites, Compos. Part A: Appl. Sci. Manuf. 42 (12) (2011) 2126–2142.

[20] N. Saba, M.T. Paridah, M. Jawaid, Mechanical properties of kenaf fibre reinforced polymer composite: a review, Constr. Build. Mater. 76 (2015) 87–96.

[21] T. Kim, S. Deveci, I. Yang, B. Stakenborghs, S. Choi, Visual, Non-destructive, and destructive investigations of polyethylene pipes with inhomogeneous carbon black distribution for assessing degradation of structural integrity, Polymers 14 (5) (2022) 1067.

[22] G. Pircheraghi, A. Sarafpour, R. Rashedi, K. Afzali, M. Adibfar, Correlation between rheological and mechanical properties of black PE100 compounds-Effect of carbon black masterbatch, Express Polym. Lett. 11 (8) (2017).

[23] A. Chudnovsky, Slow crack growth, its modeling and crack-layer approach: a review, Int. J. Eng. Sci. 83 (2014) 6–41.

[24] A. Almomani, A.H.I. Mourad, S. Deveci, J.W. Wee, B.H. Choi, Recent advances in slow crack growth modeling of polyethylene materials, Mater. Des. (2023) 111720.

[25] R. Schouwenaars, V.H. Jacobo, E. Ramos, A. Ortiz, Slow crack growth and failure induced by manufacturing defects in HDPE-tubes, Eng. Fail. Anal. 14 (6) (2007) 1124–1134.

[26] V. Favier, T. Giroud, E. Strijko, J.M. Hiver, C. G'sell, S. Hellinckx, A. Goldberg, Slow crack propagation in polyethylene under fatigue at controlled stress intensity, Polymer 43 (4) (2002) 1375–1382.

[27] M. Haager, G. Pinter, R.W. Lang, Estimation of slow crack growth behavior in polyethylene after stepwise isothermal crystallization, Macromol. Symp. 217 (2004) 383–390.

[28] M. Nie, S. Bai, Q. Wang, High-density polyethylene pipe with high resistance to slow crack growth prepared via rotation extrusion, Polym. Bull. 65 (2010) 609–621.

[29] C. Domínguez, N. Robledo, B. Paredes, R.A. García-Muñoz, Strain hardening test on the limits of slow crack growth evaluation in high resistance polyethylene resins: effect of comonomer type, Polym. Test. 81 (2020) 106155.

[30] Y. Zhang, A. Xiang, X. Lu, H. Zhou, D. Yin, H. Tian, Research on slow crack growth resistance of polyethylene pipe based on strain hardening modulus, J. Vinyl Addit. Technol. 28 (1) (2022) 226–234.

[31] F. Gholami, G. Pircheraghi, A. Sarafpour, Long-term mechanical performance of polyethylene pipe materials in presence of carbon black masterbatch with different carriers, Polym. Test. 91 (2020) 106857.

[32] M. Ahadi, M.S. Bakhtiar, Leak detection in water-filled plastic pipes through the application of tuned wavelet transforms to acoustic emission signals, Appl. Acoust. 71 (7) (2010) 634–639.

[33] T. Hashimoto, M. Takenaka, K. Aizawa, N. Amino, M. Nakamura, S. Koizumi, New insight into hierarchical structures of carbon black dispersed in polymer matrices: a combined small-angle scattering study, Macromolecules 41 (2) (2008) 453–464.

[34] R. Davand, S. Hassanajili, M.R. Rahimpour, R. Rashedi, A. Sepahi, S. Hosseini, K. Valieghbal, The UV stability of polyethylene pipes with different comonomer content: effect of carbon black masterbatch, Polym. Eng. Sci. 62 (10) (2022) 3194–3205.

[35] J. Beauson, G. Schillani, L. Van der Schueren, S. Goutianos, The effect of processing conditions and polymer crystallinity on the mechanical properties of unidirectional self-reinforced PLA composites, Compos. Part A: Appl. Sci. Manuf. 152 (2022) 106668.

[36] N.Y. Ning, Q.J. Yin, F. Luo, Q. Zhang, R. Du, Q. Fu, Crystallization behavior and mechanical properties of polypropylene/halloysite composites, Polymer 48 (25) (2007) 7374–7384.

[37] Z. Xie, D. Liu, Y. Xiao, K. Wang, Q. Zhang, K. Wu, Q. Fu, The effect of filler permittivity on the dielectric properties of polymer-based composites, Compos. Sci. Technol. 222 (2022) 109342.

[38] B.A. Schrauwen, R.P. Janssen, L.E. Govaert, H.E. Meijer, Intrinsic deformation behavior of semicrystalline polymers, Macromolecules 37 (16) (2004) 6069–6078.

[39] B.J. Carey, P.K. Patra, L. Ci, G.G. Silva, P.M. Ajayan, Observation of dynamic strain hardening in polymer nanocomposites, ACS Nano 5 (4) (2011) 2715–2722.

[40] G. Basseri, M. Mehrabi Mazidi, F. Hosseini, M.K. Razavi Aghjeh, Relationship among microstructure, linear viscoelastic behavior and mechanical properties of SBS triblock copolymer-compatibilized PP/SAN blend, Polym. Bull. 71 (2014) 465–486.

[41] S. Trinkle, P. Walter, C. Friedrich, Van Gurp-Palmen plot II–classification of long chain branched polymers by their topology. Rheol. Acta 41 (1) (2002) 103–113.

[42] J.F. Vega, J. Martinez-Salazar, M. Trujillo, M.L. Arnal, A.J. Muller, S. Bredeau, P. Dubois, Rheology, processing, tensile properties, and crystallization of polyethylene/carbon nanotube nanocomposites, Macromolecules 42 (13) (2009) 4719–4727.

[43] T. Wu, L. Yu, Y. Cao, F. Yang, M. Xiang, Effect of molecular weight distribution on rheological, crystallization and mechanical properties of polyethylene-100 pipe resins, J. Polym. Res. 20 (2013) 1–10.

[44] F. Gholami, G. Pircheraghi, R. Rashedi, A. Sepahi, Correlation between isothermal crystallization properties and slow crack growth resistance of polyethylene pipe materials, Polym. Test. 80 (2019) 106128.

[45] J.J. Zeng, W.Y. Gao, Z.J. Duan, Y.L. Bai, Y.C. Guo, L.J. Ouyang, Axial compressive behavior of polyethylene terephthalate/carbon FRP-confined seawater sea-sand concrete in circular columns, Constr. Build. Mater. 234 (2020) 117383.

[46] Y. Jiang, S. Zhang, Experimental and analytical study on the mechanical properties of rubberized self-compacting concrete, Constr. Build. Mater. 329 (2022) 127177.

[47] W. Li, Y. Xie, K. Ma, G. Long, N. Li, H. Zhao, The properties and meso/microstructure characteristics of interfacial zone between precast concrete and self-compacting concrete, Constr. Build. Mater. 297 (2021) 123753.

[48] S. Deveci, D. Fang, Correlation of molecular parameters, strain hardening modulus and cyclic fatigue test performances of polyethylene materials for pressure pipe applications, Polym. Test. 62 (2017) 246–253.